

New light on Dark Cosmos

Enrique Gaztañaga¹, Marc Manera¹, Tuomas Multamäki²

¹ Institut d'Estudis Espacials de Catalunya, IEEC/CSIC, F. de Ciencies, Torre C5 Par 2a, UAB, Bellaterra (08193 BARCELONA)

² NORDITA, Blegdamsvej 17, DK-2100, Copenhagen, Denmark

2 December 2024

ABSTRACT

Recent studies by a number of independent collaborations, have correlated the CMB temperatures measured by the WMAP satellite with very different galaxy surveys that trace the matter distribution with the whole range of the electromagnetic spectrum: radio, far-infrared, optical and X-ray surveys. The new data systematically finds positive correlations, indicating a rapid slow down in the growth of structure in the universe. Individual cross-correlation measurements are of low significance, but we show that combining data at different redshifts introduces important new constraints. Contrary to what happens at low redshifts, for a fixed Ω_m , the higher the dark energy contend, Ω_Λ , the lower the ISW cross-correlation amplitude. At 68% confidence level, the data finds independent evidence of dark energy ($\Omega_\Lambda = 0.3 - 1.0$). It also confirms, to higher significance, the presence of a large dark matter component ($\Omega_m = 0.15 - 0.35$) exceeding the density of baryonic matter, but far from the critical value. The universe seems to be dominated by dark energy and by (non-baryonic) dark matter, both of yet unknown nature.

1 INTRODUCTION

In the last few years a new cosmological scenario with a significant smooth Dark Energy (DE) component has emerged. The Cosmic Concordance Model (CCM, from now on) is a spatially flat universe with baryons ($\Omega_b \sim 4\%$), cold dark matter ($\Omega_m \sim 23\%$) and a significant DE component ($\Omega_\Lambda \sim 73\%$). The model is well supported by the supernova type Ia (SNIA) observations (Riess et al. 1998; Perlmutter et al. 1999), large scale structure (LSS) measurements (Tegmark et al. 2004; Percival et al. 2001) and the cosmic microwave background experiments (CMB), in particular by the recent WMAP experiment (Bennett et al. 2003). The energy density of the universe seems dominated by the unknown DE component, presenting a formidable observational and theoretical challenge. The three key observational probes measure complementary aspects of the cosmological parameter space. The SNIA indicate that the universe is accelerating but present data is degenerate for alternative cosmological scenarios (see Fig. 3). The LSS observations constrain Ω_m but leave the DE question unanswered. Constraints from primary anisotropies in the CMB indicate that we live in a flat universe but require a prior on the value of the local Hubble rate H_0 (Blanchard 2003). Assuming that the universe is well described by a Λ CDM model, combining all these three observations gives us the cosmological CCM model.

The Integrated Sachs Wolfe effect, ISW, (Sachs & Wolfe 1967) is a direct probe for the (linear) rate of structure formation in the universe. Secondary anisotropies in the CMB

appear because of the net gravitational redshifts affecting CMB photons that travel through an evolving gravitational potential Φ . These secondary temperature anisotropies are therefore correlated with local, evolving, structures on large scales. The correlation is negative when structures grow, as increasing potential leaves a cold spot in the CMB sky, and positive otherwise. In a flat universe without DE (Einstein-deSitter, or EdS, model) this cross-correlation is expected to be zero because the gravitational potential remains constant, despite the linear growth of the matter fluctuations.

The rate of structure formation in the universe can also be measured by galaxy peculiar velocities or galaxy redshift distortions, on very large scales through the so-call β parameter determination (Peacock et al. 2001; Pope et al. 2004). The ISW effect provides an independent and complementary probe of the same effect. Independent, because it uses temperature anisotropies instead of the velocity field, and complementary, because of the different assumptions and systematics that relate measurements with theory. Despite recent advances in the size of galaxy redshift surveys such as SDSS and 2dFGRS, the spectrum of matter fluctuations $P(k) \propto <\delta(k)^2>$ is quite difficult to measure directly over very large scales (Tegmark et al. 2004; Percival et al. 2001; Gaztañaga & Baugh 1998). Part of the problem is that matter correlations fall quickly to zero on scales larger than 30 Mpc/h ($k < 0.1 \text{ h/Mpc}$). In contrast, fluctuations in the gravitational potential go as $\Phi(k) \propto \delta(k)/k^2$ so that they fall less rapidly with scale (see comments to Fig. 2). The ISW cross-correlation traces the gravitational potential, Φ , and thus provides a new window to study the largest structures,

extending over several degrees in the sky or many tens of Mpc/h at the survey depth.

2 GROWTH OF DENSITY PERTURBATIONS

Gravitational evolution of matter fluctuations, $\delta = \rho/\bar{\rho} - 1$, is dependent on the cosmological model via the evolution of the scale factor $a = a(t)$. Compared to a static background, a rapidly expanding background will slow down the collapse of an over dense region. In the linear regime, a small initial perturbation δ_0 grows according to the growth factor $D(t)$:

$$\delta(t) = D(t) \delta_0. \quad (1)$$

Under generic assumptions, (Gaztañaga & Lobo 2001; Multamäki, Gaztañaga & Manera 2003; Lue, Scoccimarro & Starkman 2004), D follows a simple harmonic equation:

$$\frac{d^2 D}{d\eta^2} + \left(2 + \frac{\dot{H}}{H^2}\right) \frac{dD}{d\eta} + 3c_1 D = 0, \quad (2)$$

where $\eta = \ln(a)$ is the conformal time and $H = H(\bar{\rho}) \equiv \dot{a}/a$ is the background Hubble rate (\dot{a} and \dot{H} are proper time derivatives). For a flat cosmological model containing DE ($w = -1$) we have: $H^2 = H_0^2(\Omega_m a^{-3} + \Omega_\Lambda)$ and $c_1 = -(1/2) \Omega_m/(\Omega_m + \Omega_\Lambda a^3)$, where Ω_Λ and Ω_m are the dark energy and dark matter densities today in units of the critical density $\rho_c \equiv 3 H^2/(8\pi G)$. In the EdS model: $\Omega_\Lambda = 0$, $\Omega_m = 1$, in which case the solution to Eq. (2) is $D \propto a$. This means that δ grows linearly with the scale factor, $\delta \propto a$, while the corresponding gravitational potential fluctuation, $\Phi \sim \delta/a$, remains constant as the universe expands.

2.1 The ISW effect

ISW temperature anisotropies are given by (Sachs & Wolfe 1967):

$$\Delta_T^{ISW}(\hat{n}) \equiv \frac{T(\hat{n}) - T_0}{T_0} = -2 \int dz \frac{d\Phi}{dz}(\hat{n}, z) \quad (3)$$

where Φ is the Newtonian gravitational potential at redshift z . One way to detect the ISW effect is to cross-correlate temperature fluctuations with galaxy density fluctuations projected in the sky (Crittenden & Turok 1996). On large linear scales and small angular separations, the cross-correlation $w_{TG}^{ISW}(\theta) \equiv \langle \Delta_T^{ISW}(\hat{n}_1) \delta_G(\hat{n}_2) \rangle$ is (Fosalba & Gaztañaga 2004):

$$\begin{aligned} w_{TG}^{ISW}(\theta) &= \frac{1}{2\pi} \int \frac{dk}{k} P(k) g(k\theta) \\ g(k\theta) &= \int dz W_{ISW}(z) W_G(z) \frac{H(z)}{c} J_0(k r_A \theta) \\ W_{ISW}(z) &= 3\Omega_m (H_0/c)^2 \frac{d[D(z)/a]}{dz} \\ W_G(z) &= b(z) \phi_G(z) D(z), \end{aligned} \quad (4)$$

where J_0 is the zero order Bessel function, ϕ_G is the survey galaxy selection function along the line of sight z and

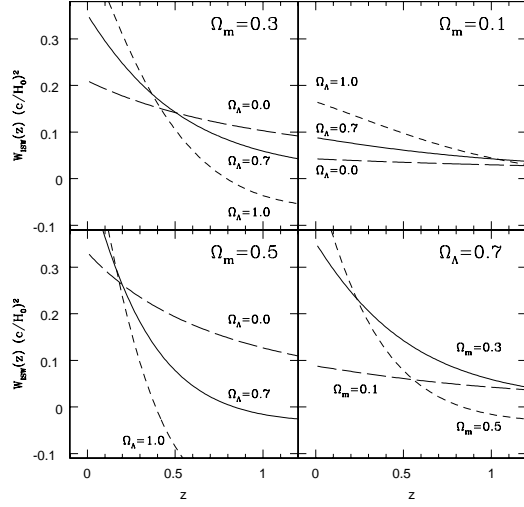


Figure 1. Redshift dependence of $W_{ISW}(z)$ in Eq.[4] for different values of Ω_m and Ω_Λ . Bottom left, top right and top left panels shows a fixed $\Omega_m = 0.5$, $\Omega_m = 0.3$ and $\Omega_m = 0.1$ respectively. In all cases: $\Omega_\Lambda = 0.0$ (short-dashed line), $\Omega_\Lambda = 0.7$ (continuous line) and $\Omega_\Lambda = 1.0$ (long-dashed line). Bottom right panel shows a fixed $\Omega_\Lambda = 0.7$ and $\Omega_m = 0.3$ (continuous line), $\Omega_m = 0.5$ (short-dashed line) and $\Omega_\Lambda = 0.1$ (long-dashed line).

$r_A = r_A(z)$ the comoving transverse distance. We make the common assumption that galaxy and matter fluctuations are related through the linear bias factor, $\delta_G(\hat{n}, z) = b(z)\delta_m(\hat{n}, z)$. For the Λ CDM case the ISW effect is non-zero, and the kernel W_{ISW} can be well approximated by $W_{ISW}(z) = -3\Omega_m (H_0/c)^2 D(z)(f - 1)$, where f is the relative growth factor, $f \simeq \Omega_m(z)^{6/11}$. The power spectrum is $P(k) = A k^{n_s} T^2(k)$, where $n_s \simeq 1^1$ and $T(k)$ is the Λ CDM tranfer function, which we evaluate using the fitting formulae of Einseinstein & Hu 1998. W_{ISW} decreases as a function of increasing redshift and goes to zero both for $\Omega_m \rightarrow 0$ and for $\Omega_m \rightarrow 1$. At low redshifts, the ISW effect is larger for larger values of Ω_m , but the redshift evolution depends on the curvature (ie how quickly the H and D evolve to the EdS case). This is illustrated in Fig.1 which shows how W_{ISW} depends on z for different values of Ω_Λ and Ω_m . At high redshifts, the lower the value of Ω_Λ (for a fixed Ω_m) the larger the ISW amplitude.

2.2 Biasing

Linear bias is used to study how well light traces the underlying statistics of linear matter fluctuations. On these very large scales, fluctuations δ are small and linear theory works well both for biasing and gravity. We remove the effects of biasing in our parameter estimation by comparing the observed galaxy-galaxy correlation w_{GG} to the matter-matter correlation w_{mm} predicted by each model

¹ Throughout the paper we made the assumption of scale invariant primordial fluctuations ($n_s \simeq 1$). For other possibilities see, eg, (Barriga et al 2001).

(Fosalba, Gaztañaga & Castander 2003). The effects of bias are also redshift dependent. The galaxy selection function we use $\phi_G(z) \sim z^2 \exp[-(z/\bar{z})^{1.5}]$, picks at $z = \bar{z}$, and we should approximate the bias with a constant $b = b(\bar{z})$ for that particular survey. We then have: $w_{TG} = b(\bar{z})w_{Tm}$ and $w_{GG} = b^2(\bar{z})w_{mm}$, so that an effective linear bias b can be estimated as the square root of the ratio of galaxy-galaxy and matter-matter correlation functions:

$$b = \sqrt{\frac{w_{GG}}{w_{mm}}}. \quad (5)$$

Such prescription has been shown to work well in a variety of galaxy models (eg see (Berlind, Narayan & Weinberg 2001)). The values of w_{mm} can be computed with Eq. (4) by just replacing $P(k)$ by $k^2 P(k)$ and $W_G W_{ISW}$ by $W_m^2 \equiv (D(z)\phi_G(z))^2$. Note how this estimation of b depends on the normalization of w_{mm} . We choose to normalize each model by fixing σ_8 . To make our results independent of this normalization we marginalize over σ_8 in a range $\sigma_8 = 0.6 - 1.2$. This is equivalent to a marginalization over the corresponding values of b . We will also marginalize over h in a range $h = 0.6 - 0.8$. We choose to compare the predictions with the raw data w_{TG} normalized to the bias in the CCM model, ie w_{TG}/b , where b is estimated for each sample using Eq.(5) with w_{mm} in the CCM model. We consequently need to renormalize each of the model predictions to the CCM model bias: $w_{TG}^{mod}/b = b_r w_{Tm}^{mod}$, where $b_r^2 = w_{mm}/w_{mm}^{mod}$ is the ratio of the concordance model prediction to the one in the corresponding model. We choose to estimate this relative bias at $R = 8$ Mpc/h, but the actual number has little effect in our final conclusions.

3 OBSERVATIONAL DATA

Recent analysis by independent collaborations, have cross-correlated the CMB anisotropies measured by WMAP with different galaxy surveys. The mean galaxy redshifts expand over a decade (ie $0.1 < \bar{z} < 1.0$) and trace the matter distribution with light from the whole range of the electromagnetic spectrum: radio, far-infrared, optical and X-ray surveys (see Table 1). The cross-correlation and error estimation techniques used are also quite different but they yield comparable results over the scales of interest (eg compare Montecarlo errors to jackknife errors in Fig.3 in (Fosalba & Gaztañaga 2004)). In our compilation of the different data sets, we average the results on fixed angular scales around $\theta = 6^\circ$. This corresponds to proper distances of $\simeq 25$ Mpc/h at $\bar{z} \simeq 0.1$ and $\simeq 100$ Mpc/h at $\bar{z} \simeq 1.0$ in the CCM model and avoids possible contamination from the small scale SZ and lensing effects (eg see Fig. 3 in (Fosalba, Gaztañaga & Castander 2003)).

Radio galaxies from NVSS (Condon et al. 1998) and hard X-ray background observed by HEAO-1 (Boldt 1987), have been cross-correlated with WMAP data (Boughn & Crittenden 2004a; Boughn & Crittenden 2004b), to find a signal of $1.13 \pm 0.35 \mu K$ relative to the CCM model prediction at $z \sim 0.9$. The different biases for X-rays, $b^2 = 1.12$, (Boughn & Crittenden 2003) and for radio galaxies, $b = 1.3 - 1.7$, (Boughn & Crittenden 2002) have been taken

into account. A compatible signal has also been found with the NVSS data by the WMAP team (Nolta et al. 2004).

The cross correlation of WMAP with galaxies ($17 < b_J < 20$) in the APM Galaxy Survey (Maddox et al. 1990) (covering about 20% of the South Galactic Cap, SGC) was found to be $w_{TG} = 0.35 \pm 0.13 \mu K$ at scales $\theta = 4 - 10^\circ$ with $b \simeq 1$ (Fosalba & Gaztañaga 2004). The cross-correlation with the SDSS DR1 (Tegmark et al. 2004) (covering about 10% of the North Galactic Cap, NGC) can be found in (Fosalba, Gaztañaga & Castander 2003). The first sample ($\bar{z} \sim 0.3$) contains ~ 5 million objects classified as galaxies in SDSS (with $r < 21$ and low associated error). For this sample, which has $b \simeq 1$, $w_{TG} = 0.26 \pm 0.13 \mu K$ at scales $\theta = 4 - 10^\circ$. The high redshift sample ($z \sim 0.5$) has $w_{TG} = 0.53 \pm 0.21 \mu K$ and $b^2 \simeq 6$. The SDSS data has also been cross-correlated with WMAP by the SDSS team (Scranton et al. 2003) using nearly 25 million galaxies in four redshift samples. Their results are compatible/comparable with those obtained in (Fosalba, Gaztañaga & Castander 2003) but no bias from galaxy-galaxy auto correlation function is given. The infrared 2MASS Galaxy Survey (Jarret et al. 2000), with $z \sim 0.1$, show a WMAP cross-correlation of 1.53 ± 0.61 times the CCM prediction, with a bias of $b = 1.18$ (Afshordi, Loh & Strauss 2004).

The data is summarized in Table 1 and displayed in Fig.1. We chose the values of NVSS+HEAO-1 quoted by (Boughn & Crittenden 2004b) as representative of both the (Nolta et al. 2004) and (Boughn & Crittenden 2004a) analysis. For the SDSS, we chose the values in (Fosalba & Gaztañaga 2004) where the CCM bias b is estimated using Eq.(5). Note how the selected samples are complementary. The samples which have large sky overlap (eg 2MASS and NVSS+HEAO-1) have negligible redshift overlap. When the redshift overlap is significant (ie in 2MASS-APM or SDSS-NVSS could be up to 20%) the sky overlap is small (less than 10%). Consequently, the different samples in Table 1 have less than 1% volume in common. This is negligible, given that individual sampling errors (which are proportional to volume) are of the order of 30%.

The most significant detection in Table 1 seems to be the one quoted by (Boughn & Crittenden 2004b) for the NVSS+HEAO-1 samples. Given the systematic uncertainties involved in the bias and selection function of both of these samples, we have checked that our results do not change much (less than 20% in the area of the contours in Fig.3) when we double the quoted errorbar. Doubling this errorbar corresponds to an additional 50% systematic uncertainty in the value b or to a 40% uncertainty in the mean redshift of the samples. The observational data not included in Table 1 is in good agreement with the values in the table, but is excluded to avoid redundancy. The agreement of the redundant data provides further confirmation and indicates that errors are dominated by sampling rather than by the methodology or the systematics.

4 RESULTS

Fig.2 compares the w_{TG} observations with predictions for a fixed value of $\Omega_m = 0.3$ and three different values of Ω_Λ .

\bar{z}	w_{TG}/b	b	catalog, Band
0.1	0.70 ± 0.32	1.1	2MASS, infrared ($2\mu m$)
0.15	0.35 ± 0.17	1.0	APM, optical (b_j)
0.3	0.26 ± 0.14	1.0	SDSS, optical (r)
0.5	0.216 ± 0.096	2.4	SDSS high-z, optical (r +colors)
0.9	0.043 ± 0.015	1-2	NVSS+HEAO, Radio & X-rays

Table 1. Observed cross correlation w_{TG}/b (averaged for $\theta \simeq 4 - 10^\circ$) of WMAP anisotropies with different catalogs. Error in w_{TG}/b includes 20% uncertainty in b .

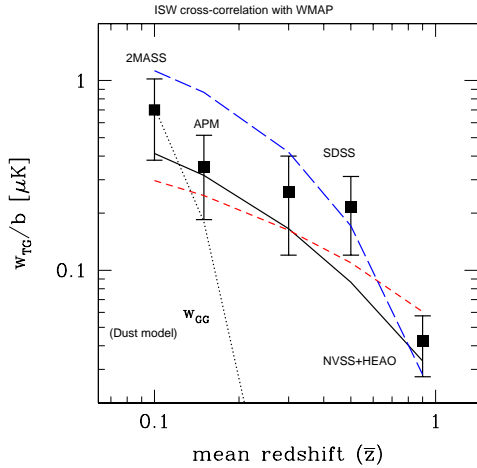


Figure 2. Symbols with error bars correspond to the different measurements w_{TG}/b in Table 1. The continuous, short-dashed and long-dashed lines show the concordance ($\Omega_m = 0.3, \Omega_\Lambda = 0.7$), opened ($\Omega_m = 0.3, \Omega_\Lambda = 0.0$) and closed ($\Omega_m = 0.3, \Omega_\Lambda = 1.1$) model predictions (at $\theta = 6^\circ$). The dotted line corresponds to the galaxy-galaxy prediction (and also the dust contamination model) with arbitrary normalization.

We can see how the shape of the prediction depends on the amount of dark energy. Even though W_{ISW} at $z = 0$ depends only weakly on Ω_Λ , the evolution with redshift depends more strongly on Ω_Λ . For a fixed Ω_m , models with larger values of Ω_Λ evolve more rapidly with redshift to the EdS case, where the ISW effect vanishes. Thus, contrary to what happens at $z = 0$, the lower the value of Ω_Λ (for a fixed Ω_m) the larger the ISW amplitude at high redshifts (see also Fig.1).

To test model predictions with the data, we use a standard χ^2 -test, $\chi^2 = \sum_i (O_i - T_i)^2 / \sigma_i^2$, where O_i and σ_i correspond to the different measurements and errors (column 2 in Table 1) and T_i correspond to the model. The label i runs for $i = 1$ to $i = 5$ marking the different redshifts (column 1 in Table 1). We use the relative χ^2 values, $\chi^2 - \chi^2_{min}$, to define confidence levels in parameter estimation. Taking $T_i = 0$ we evaluate the significance of the combined ISW detection. We find that this null hypothesis is rejected with a very high probability: $P \simeq 99.997\%$ (from $P_{\nu=4}(\chi^2 > 26) \simeq 3 \times 10^{-5}$). We next compute the expected ISW effect and compare it with the observational data within the Λ CDM family of

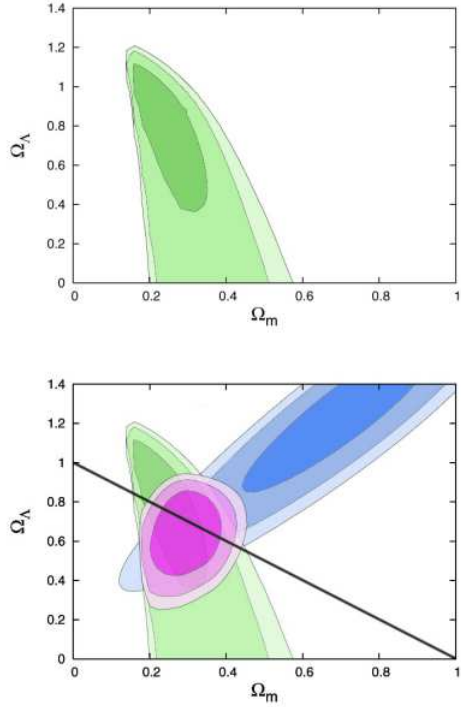


Figure 3. 68, 95 and 99% confidence contours in the $(\Omega_m, \Omega_\Lambda)$ plane (marginalized over h) for the Λ CDM model. Top: constraints from only ISW. Bottom: constraints from SNIa (blue) and ISW (green) along with the combined contours (purple).

models, where Ω_m , Ω_Λ and h^2 are free parameters (we fix the baryonic content $\Omega_b \simeq 0.05$ and the primordial spectral index $n_s \simeq 1$). To make our results independent of the overall matter normalization, we marginalize the probabilities over the range $\sigma_8 = 0.6 - 1.2$. This is equivalent to a marginalization over the overall value of b . As we compare w_{GT} normalized to the CCM model bias, we need to compute the relative bias for other LCDM models, as mentioned above. We also marginalized over h in a range $h = 0.6 - 0.8$.

The best fit corresponds to $\Omega_m \simeq 0.25 \pm 0.10$, $\Omega_\Lambda \simeq 0.65 \pm 0.35$, in good agreement with other cosmological probes mentioned above. In Fig. 3 we show the confidence contours for a Λ CDM model along with the constraints from recent SNIa (Barris et al. 2004) observations. From the figure it is clear how the ISW effects gives new important information about the cosmological parameters. The EdS model is ruled out to high significance. The confidence contours are almost perpendicular to the SNIa contours, allowing to constrain the model well with just these two sets of observations.

4.1 Possible Contaminants

The constraining power of the new ISW data comes from the simultaneous fitting of data at different redshifts, that

² We use $H_0 \equiv 100 h \text{ km/s/Mpc}$.

is from the shape information in Fig. 2. Because of the uncertainties in the relative normalization due to a relative bias, any given point alone does not constrain well the cosmological parameters. But the combination of the data gives us a new powerful tool for cosmological parameter estimation.

The shape of the curve as a function of redshift also provides an important test for systematics. CMB and galaxy maps are both masked and corrected from galactic absorption/extinction, but any residual contamination could produce a cross-correlation signal. Emission and absorption by our own galaxy produce patchy hot spots in the CMB maps and negative density fluctuations in the galaxy distribution (because of extinction). In principle, this should therefore result in a negative cross-correlation, but overcorrecting for the effects of galactic absorption could also result in a positive signal. This possibility have been tested for each of the samples, by comparing the cross-correlation to WMAP maps at different frequencies. Most analysis use the WMAP Kp0 mask, which excludes about 30% of sky on the basis of galactic or extra-galactic (eg radio sources) contamination. In all cases the contamination seems smaller than the errors (eg see Fig. 2 in (Fosalba & Gaztañaga 2004)). Moreover, one does not expect this effect to have any redshift dependence, contrary to the measurements in Fig. 2.

Cold dust in distant galaxies, will also produce patchy hot spots in the CMB maps and positive density fluctuations in the galaxy distribution (could also be negative because of internal extinction). The resulting cross-correlation should trace the galaxy-galaxy auto correlation function, w_{GG} , and should therefore have a very different redshift dependence to the ISW effect. The dotted line in Fig. 2 shows the predicted shape dependence for w_{GG} contamination with arbitrary normalization. The shape is clearly incompatible with the actual cross-correlation measurements. It is also worth noting how w_{GG} goes quickly to zero at $\bar{z} \simeq 0.2$, while the ISW cross-correlation remains positive. This is due to the fact that at these corresponding large scales, $\gtrsim 40$ Mpc/h, matter-matter correlations w_{mm} effectively decays to zero, while w_{TG} , which traces the gravitational potential, has a less rapid decay with distance.

5 CONCLUSION

In summary, the cross-correlation of CMB anisotropies with very different galaxy surveys provides consistent detections. Their combination follows the CCM predictions with a probability of only $\simeq 3 \times 10^{-5}$ for being a false detection. This provides new and independent evidence for dark energy and dark matter, ruling out the EdS model to a high significance (for any value of H_0). Combination with SNIA data results in strong constraints to $\Omega_m \simeq 0.30 \pm 0.05$ and $\Omega_\Lambda \simeq 0.65 \pm 0.15$, in good agreement with the flat universe $\Omega_m + \Omega_\Lambda \simeq 1$ found independently by CMB data (Bennett et al. 2003; Tegmark et al. 2004). Errors in cosmological parameters from ISW detection are no match to CMB errors, even though they will improved with future surveys (Afshordi 2004). But these new constraints rely in a totally different physical effect than those exploited in previous determinations. CMB and SNIA tests used distance indicators

and standard rulers, while traditional LSS test, based on $P(k)$, relies on the physics of the CDM transfer function. The ISW measurements presented here are mostly sensitive to the time evolution in the growth of the linear gravitational potential. We marginalize our results to make them independent of both the local Hubble constant (h) and the overall rms amplitude of fluctuations (σ_8 or b). The observational data shows, for the first time, statistical evidence of a slow down in structure formation on the largest scales, $25 - 100$ Mpc/h, reached so far.

ACKNOWLEDGEMENTS

Acknowledgements: We acknowledged support from the Spanish Ministerio de Ciencia i Tecnologia, project AYA2002-00850 with EC-FEDER funding, and from the Catalan Departament d'Universitats, Recerca i Societat de la Informaci.

REFERENCES

Afshordi, N. , Loh, Y., Strauss, M. A., 2004, Phys. Rev. D 69, 083524
 Afshordi, N., 2004 astro-ph/0401166.
 Barriga, J., Gaztañaga, E., Santos, M.G., Sarkar, S., 2001, MNRAS 324, 977
 Barris, B. J. et al., 2004, ApJ 602, 571.
 Bennett C.L. et al., 2003, ApJ Suppl., 148,1
 Berlind, A., Narayan, V., Weinberg, D., 2001, ApJ 549, 688
 Blanchard, A., Douspis, M., Rowan-Robinson, M., Sarkar, S., 2003, A&A, 412, 35.
 Boldt, E., 1987, Phys. Rep. 146, 215.
 Boughn, S., Crittenden, R. 2004, Nature 427, 45
 Boughn, S., Crittenden, R. 2004, astro-ph/0404470
 Boughn, S., Crittenden, R. 2003, astro-ph/0305001
 Boughn, S., Crittenden, R. 2002, Phys. Rev. Lett. 88, 021302
 Condon J. J. et al., 1998, AJ 115, 1693
 Crittenden, R. G. Turok, N., 1996, Phys. Rev. Lett. 76, 575.
 Einseinstein, D.J. & Hu, W. 1998, Astrophys. J. 496, 605
 Fosalba, P. Gaztañaga, E., 2004, MNRAS 350, 37
 Fosalba, P. Gaztañaga, E., Castander, F.J., 2003, ApJ 597, L89
 Gaztañaga, E. & Baugh, C. M., 1998, MNRAS, 294, 229
 Gaztañaga, E., & Lobo, J. A., 2001, ApJ 548, 47
 Jarret, T. H., et al., 2000, AJ 119, 2498
 Lue, A., Scoccimarro, R., Starkman, G., 2004, Phys. Rev. D, 69, 044005
 Maddox, S. J. ,Efstathiou, G., Sutherland, W. J., Loveday, J., 1990, MNRAS 242, 43P
 Multamäki, T., Gaztañaga, R., Manera, M., 2003, MNRAS 334, 761
 Nolta, M. R. et al. 2004, ApJ 608, 10
 Peacock, J. A. et al., 2001, Nature, 410, 169
 Percival W.J. et al., 2001, MNRAS, 327, 1297
 Perlmutter, S. et al., 1999, ApJ 517, 565
 Pope, A. C. et al., 2004, ApJ, 607, 655
 Riess A. G. et al., 1998, AJ 116, 1009
 Sachs, R. K., Wolfe, A. M., 1967, ApJ 469, 437
 Scranton, R. et al., 2003 astro-ph/0307335.
 Sugiyama, N., 1995, ApJ Suppl. 100, 281
 Tegmark, M. et al., 2004, ApJ, 606, 70